Available online at www.sciencedirect.com
ScienceDirect
Trans. Nonferrous Met. Soc. China 35(2025) 4137−4148
Transactions of Nonferrous Metals Society of China
www.tnmsc.cn

Effects of deformation states on evolution of microstructures and mechanical properties in diffusion bonded TC4 alloys by hot bending

Can LI[1], Yong LI[1], De-xin ZHANG[1], Yan-qiang XU[2], Xiao-xing LI[1], Guang-lu MA[2]

1. School of Mechanical Engineering and Automation, Beihang University, Beijing 100191, China;
2. AECC Shenyang Liming Aero-engine CO. LTD, Shenyang 110043, China

Received 8 April 2024; accepted 16 December 2024

Abstract: The effects of various hot deformation states on the evolution of microstructures and mechanical properties in diffusion bonded TC4 alloys were investigated using the hot bending of thick plates. Finite element simulations were conducted to characterize the deformation states during bending at 750 °C with angles of 17° and 32°. The microstructures and mechanical properties of the bonding interface were then analyzed. The joint subjected to uniaxial stress exhibited the highest ultimate tensile strength, which was attributed to the significant accumulation of dislocation density and the low-angle grain boundaries within the grains. The texture strengthening in the basal {0001} plane was also observed, along with a relatively low Schmid factor corresponding to the primary slip systems aligned with the deformation direction. In contrast, the joint under stress-free conditions showed a slip direction that was less favorable for deformation, resulting in an ultimate tensile strength higher than that of the joint under biaxial stress conditions.
Key words: diffusion bonded joint; thick plate; hot bending; stress state; tensile strength

1 Introduction

Diffusion bonding has been widely used in the fabrication of titanium alloy components with complex internal geometries, such as aero-engine blades and microchannel heat exchangers [1,2]. Typically, the diffusion bonded (DB) titanium alloy plates undergo additional hot forming processes to achieve the final shapes, such as the hot bending, twisting, and superplastic forming for the aeroengine blades [3]. Since these components generally suffer from harsh service environments, including heavy load and extreme ambient temperature, mechanical properties of the DB joint must be preserved following these subsequent forming operations [4]. Consequently, a comprehensive investigation into how various deformation states affect the microstructures and resulting mechanical properties is essential for ensuring the performance and reliability of these critical components.

Many studies have investigated the welding parameters to enhance the performance of DB joints, focusing on bonding stress, temperature, and holding time [5]. The post-processes can be summarized as post-weld heat treatment (PWHT) and post-weld heat deformation (PWHD). ZHANG et al [6] demonstrated that PWHT could increase the impact toughness of the TC4 DB joint due to grain boundary migration. DZIADOŃ and MUSIAŁ [7] proved that the strength properties of post-weld aged AZ91 laser welded joint were much worse than the welded material. The above studies about the effect of PWHT on the properties of welded joints are often related to interface migration and grain growth. LI et al [8] found that different hot tensile conditions led to a remarkable difference in

Corresponding author: Yong LI, Tel: +86-18811787363, E-mail: liyong19@buaa.edu.cn
https://doi.org/10.1016/S1003-6326(25)66934-2

dynamic softening performance between the TC4 DB joint and heat-treated base metal. The plasticity of the TC4 DB joint during the tensile process was damaged by very few tiny voids at the bonding interface. JIANG et al [9] showed that the post-weld tensile deformation retarded the ductility degradation of the reeled-pipeline welded joint because of the dislocation walls and cells related to the PWHD process. TANG et al [10] proved that the hot compression significantly affected the bonding interface of the TiAl/Ti2AlNb DB joint. TAN et al [11] performed isothermal compression deformation and heat treatment on the electron beam welded Ti2AlNb/TC11 joint, and the impact toughness of the joint was improved. LIU et al [12] examined that the yield strength of the ZK60 friction-stir-welded joint increased by 45 MPa after 5% post-weld compression because of the twins and dislocations generated during the compression. ZHU et al [13] investigated the influence of PWHT and hot compression on interfacial microstructure and mechanical properties of the TiAl/Ti2AlNb direct DB joint. Both post-bonded treatments can enhance the tensile properties of the joint by eliminating the brittle intermetallic compounds. The influence of hot compression on the welding interface is mainly due to dislocation and compound evolution. WAN et al [14] applied the cold bending process to the 316L stainless steel arc welded sheet, and the hardness in the welded joint increased with the increasing bending angle. Tensile and compressive residual stresses were observed on both the outer and inner surfaces of the bending sheet. However, the research on diffusion bonding is limited.

Most current studies primarily focus on simple tension or compression deformation states, which significantly differ from the typical deformation states, such as bending, used to manufacture actual parts. In this study, a hot bending method is used to obtain various deformation states in the thick DB plate efficiently, and the microstructures and mechanical properties of the DB joint are discussed.

2 Experimental

A good bonding quality of the TC4 DB plate, with a thickness of 46 mm, was obtained under the optimal bonding pressure of 2 MPa with a temperature history of 900 °C for 1 h and 930 °C for 2 h, which lays a foundation for the reliability of subsequent results.

As shown in Fig. 1(a), the DB plate was cut into thick plate samples with dimensions of 280 mm × 90 mm × 46 mm. Hot V-bending tests were conducted at 750 °C with a stamping speed of 1 mm/s. The movement displacements of the upper mold were 30 and 45 mm, respectively. Before the test, the plate and mold were spread with the boron nitride lubricant on both sides to reduce friction. After V-bending, the plate was cooled in the air. As shown in Fig. 1(b), the bending angle before springback is denoted as α_f, and the bending angle after springback is denoted as α_s. So, the springback angle is denoted as $\Delta\alpha=\alpha_f-\alpha_s$.

However, directly measuring α_f is difficult before unloading at high temperatures. According to GB/T 232—2010, the value of α_f can be determined by the displacement of the upper head, which can be expressed as

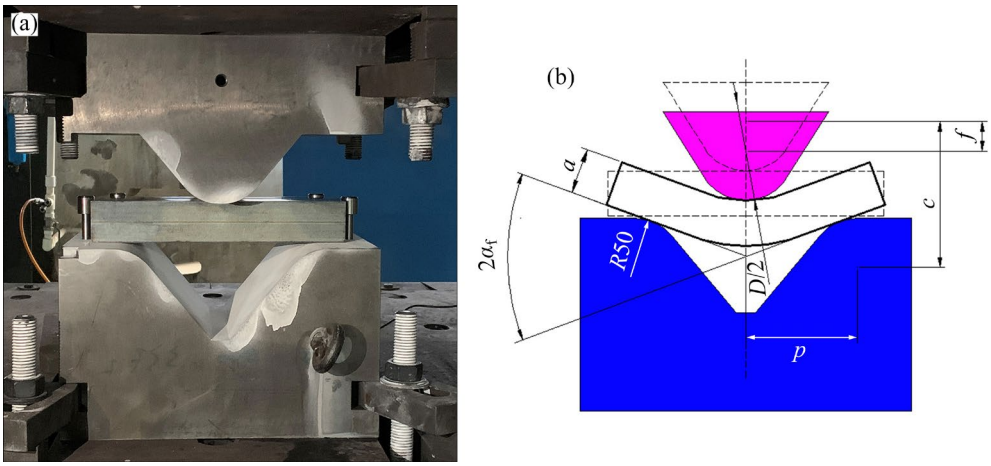

Fig. 1 Schematic diagram of hot bending experiment: (a) Hot bending die and thick sheet; (b) Hot bending process (Unit: mm)

$$\begin{cases} \sin\alpha_f = \dfrac{pc + W(f-c)}{p^2 + (f-c)^2} \\ \cos\alpha_f = \dfrac{Wp - c(f-c)}{p^2 + (f-c)^2} \\ W = \sqrt{p^2 + (f-c)^2 - c^2} \\ c = 25 + a + \dfrac{D}{2} \end{cases} \quad (1)$$

where a is the plate thickness, D is the punch diameter, p is the distance between the fillet center of the low die and the center axis of the indenter, and f is the displacement distance of the punch.

The hot-bending plate can be divided into two regions: the PWHD region with bending deformation and the PWHT region with negligible deformation, as shown in Fig. 2. The TC4 DB joints at the PWHD and PWHT regions were selected for tensile tests and microstructure characterizations. Tensile tests at RT with a tensile speed of 0.025 mm/s were conducted on an Instron Sans-100 kN universal machine. Each test was repeated four times. The geometric dimensions of tensile specimens are also shown in Fig. 2.

Microstructures of the DB joints under different states were observed using a Gemini 450 scanning electron microscope (SEM) and electron backscattering diffraction (EBSD). The samples for OM and SEM were rotary polished and etched using Kroll solution. The samples for EBSD characterization were vibratory polished. EBSD data can be used to obtain the pole figure (PF), inverse pole figure (IPF), grain boundary (GB) maps, local average misorientation (LAM) maps, and Schmid factor (SF) maps.

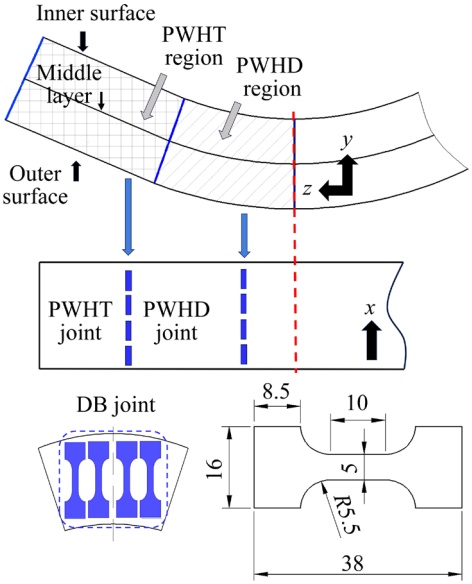

Fig. 2 Schematic diagram and dimensions of specimens for tensile test (Unit: mm)

3 Finite element simulation

A two-dimensional symmetric finite element (FE) model was established using dynamic explicit and static algorithms to simulate the hot bending and springback of the TC4 DB plate. Figure 3(a) displays the EBSD microstructure of the DB joint, which shows some variation in the thickness of the weld zone, with an average value of approximately 0.1 mm. Hence, a subsection is defined in the FE model, as illustrated in Fig. 3(b). The element meshes used in this analysis are hexahedral elastic-plastic elements. In the matrix zone, a four-node solid element with a mesh size of 1.5 mm is used, while the mesh in the weld zone consists of four layers with a mesh size of 0.025 mm.

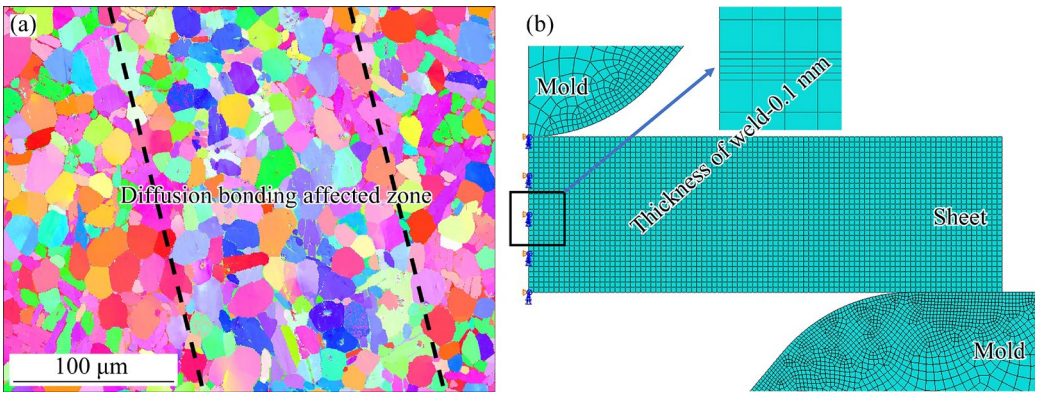

Fig. 3 Model definition of hot bending DB plate: (a) EBSD map of DB joint; (b) Schematic diagram of hot bending FE model

Table 1 Model parameters of matrix and weld zone for TC4 DB plate

Zone	Temperature/ °C	Young's modulus/MPa	Poisson's ratio	Thermal conductivity/ ($mW·mm^{-1}·°C^{-1}$)	Specific heat capacity/ ($kJ·kg^{-1}·°C^{-1}$)	Yield strength/MPa	Density/ (10^{-9} $kg·m^{-3}$)
Matrix	750	10973	0.42	14.6	717	281	4.4
Weld	750	12285	0.42	14.6	717	316	4.4

As shown in Table 1 and Fig. 4, the material parameters of the matrix zone and weld zone at 750 °C and 0.1 s^{-1} were obtained by uniaxial tensile tests. The tools were set to be rigid bodies. The bending temperature was set as 750 °C, and the friction coefficient was 0.15. Velocity boundary conditions were applied to the upper mold. The *z*-axis (Fig. 2) displacement of nodes on the symmetrical axis was set as zero.

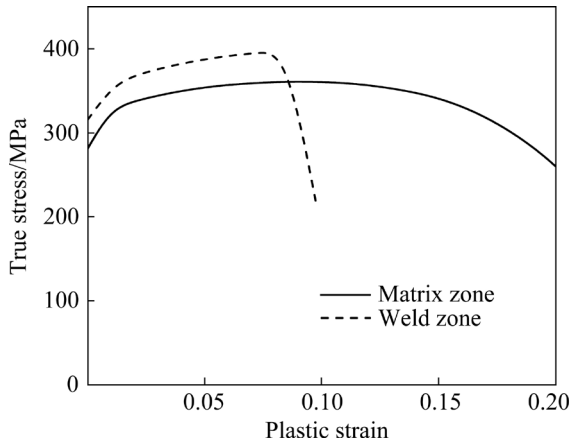

Fig. 4 True stress−plastic strain curves at 750 °C and 0.1 s^{-1}

4 Results

4.1 Deformation states

The bending angles, denoted as α_s, were measured for the thick plates, as illustrated in Fig. 5. The measured angles are 17° and 32°, respectively. The calculated values of α_f were 17.98° and 32.26° according to Eq. (1). So the springback angles are 0.98° and 0.26°, respectively. When α_s equals 17°, the thickness of the metal layer inside the weld after bending is 23 mm, and the thickness outside the weld is 21 mm. When α_s equals 32°, the corresponding thicknesses are 23.5 and 19.3 mm, respectively. According to the thick plate metal bending theory [15], the inward movement of the strain neutral layer leads to the plate thickness thinning of the deformation area (PWHD region). The experimental results agree with the theory,

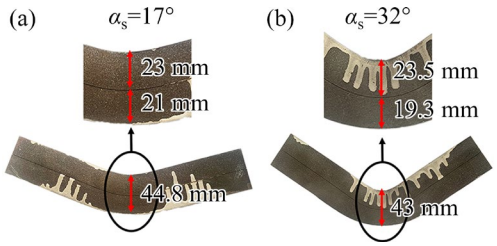

Fig. 5 Thick plate after hot-bending with different bending angles

which shows that the greater the bending angle, the greater the inward displacement of the neutral layer.

The load simulation results for the TC4 DB plate during bending are shown in Fig. 6(a). The simulated load is approximately 200 kN, matching the experimental value. The boundary curves of the cross-section for the bending plate before and after springback are extracted. The comparison results are shown in Figs. 6(b) and (c). The black solid line represents the sample before springback, while the red dotted line indicates the sample after springback. When the bending angle is 17°, the springback angle predicted by the simulation is 1.40°, which is close to the experimental results (0.98°). At a bending angle of 32°, the simulation shows a significantly small springback angle of 0.10°, which is also consistent with the experimental observation of 0.26°. These findings demonstrate the effectiveness of the simulation model.

As shown in Fig. 7(a), the distribution of equivalent stress is asymmetrical in the radial direction, which is mainly because the lowest point of the upper mold is not in contact with the plate during the subsequent forming process. The PWHD region can be subdivided into representative PWHD1 and PWHD2 regions. At the PWHD1 region, stress concentration occurs at the inner rounded corners. In contrast, the PWHD2 region exhibits relatively high stress levels that extend across the weld layer. As shown in Fig. 7(b), 35 nodes are selected along the thickness direction to obtain tangential stress (σ_t) and radial stress (σ_r). The nodes in the weld zone are numbered from No.17 to No.19.

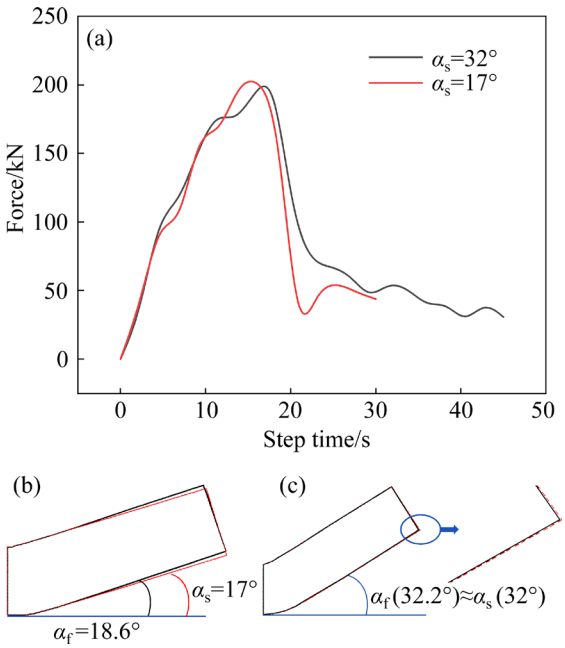

Fig. 6 Simulation results of TC4 bending DB plate: (a) Load curves; (b, c) Springback results at α_s=17° and α_s=32°, respectively

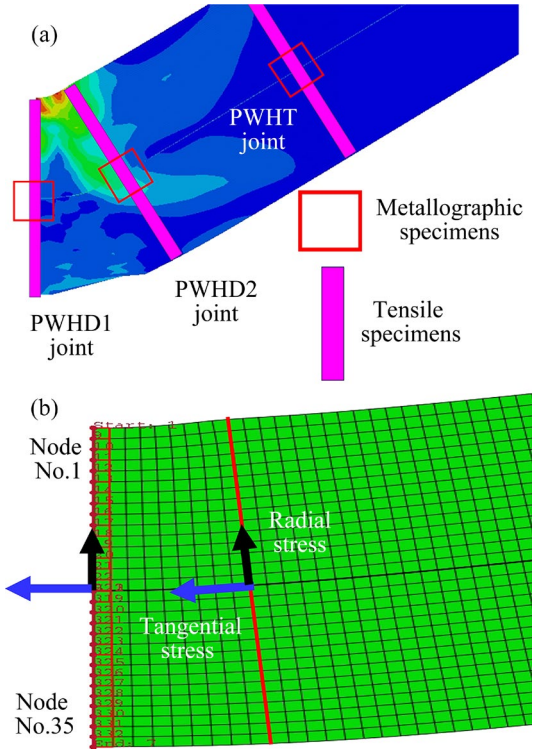

Fig. 7 Sample cutting schematic diagram of TC4 DB plate after bending

The stress distribution in the typical regions is shown in Fig. 8. As shown in Figs. 8(a) and (b), when the bending angle increases from 17° to 32°, the deformation state of the weld zone at the PWHD1 region is in a transition stage from tangential tension to compression and radial compression to tension. For the weld zone of the PWHD2 region, the tangential stress remains in a tensile state at a bending angle of 17°. The radial stress is negligible. However, when the bending angle increases to 32°, the tangential stress becomes negligible, while the radial stress remains in a compressive state. Figure 8(c) summarizes the deformation states in the weld zone obtained by bending. The stress-free state without deformation is applied to the PWHT joint. Bending causes stress

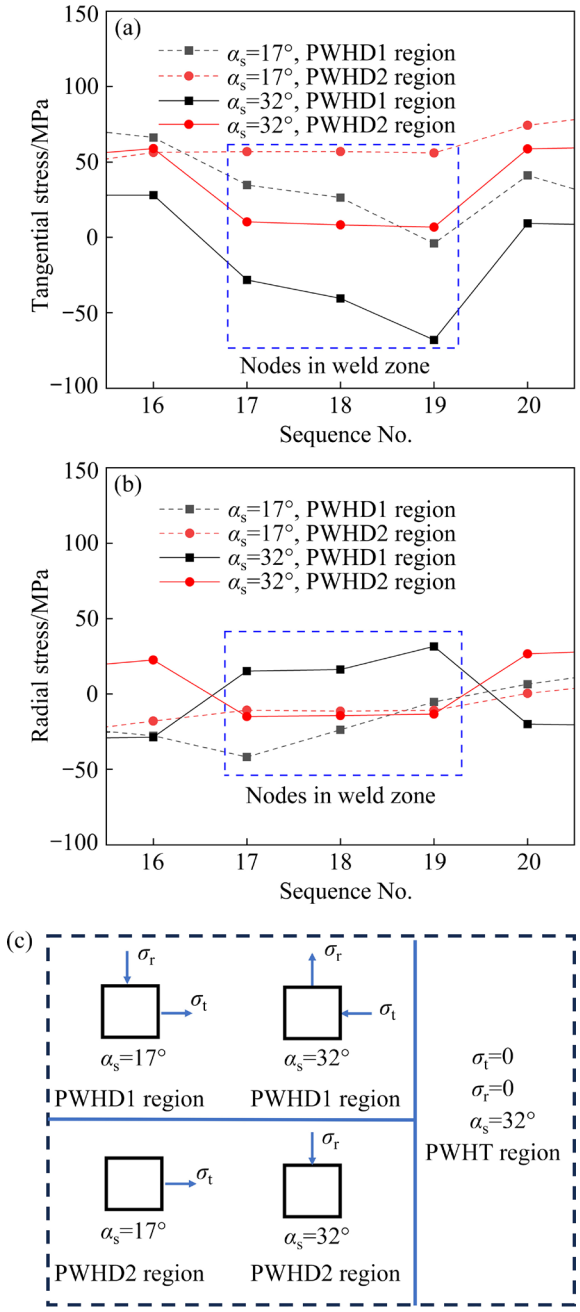

Fig. 8 Deformation states of weld zone in TC4 DB bending plates: (a) Tangential stress; (b) Radial stress; (c) Stress state in weld zone

partitioning in metal microstructure, which has been proven to cause inhomogeneous dislocation distribution [16]. The PWHD1, PWHD2 and PWHT joints with different deformation states are selected for tensile tests and metallographic observation.

4.2 Mechanical properties

The ultimate tensile strength and elongation of the DB joints are illustrated in Fig. 9. At a bending angle of 17°, the ultimate tensile strength of the joint at the PWHD1, PWHT and PWHD2 regions are 755.18, 786.25 and 820.96 MPa, respectively. At a bending angle of 32°, the ultimate tensile strength of the joint at the PWHD1, PWHT and PWHD2 regions are 706.60, 783.58 and 1177.45 MPa, respectively. The increase in tensile strength of the PWHD2 joint at a bending angle of 32° is more significant than that at a bending angle of 17°.

4.3 Microstructure evolution

4.3.1 SEM observation of DB interface

As shown in Fig. 10(a), the voids and gaps at the DB interface of the as-received (AR) joint are eliminated due to volume and surface diffusion processes. Some isolated ellipse voids remain visible at the DB interface, as shown in Figs. 10(b) and (c). These voids are often difficult to observe due to their small size. Generally, a sound joint with few defects is acceptable, and the influence of tiny voids on the mechanical properties was neglected.

Figures 10(d−f) show the DB interface of the

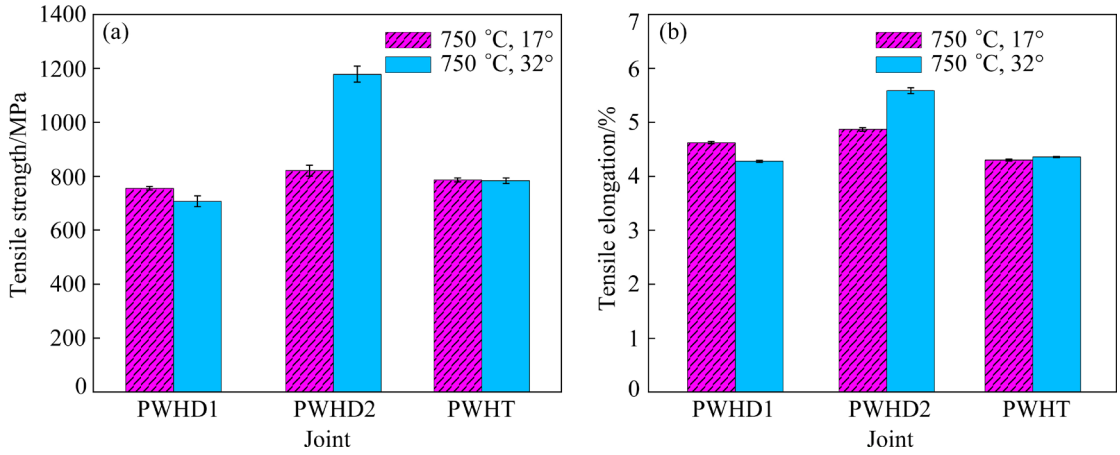

Fig. 9 Tensile properties of TC4 DB joint after hot bending: (a) Strength; (b) Elongation

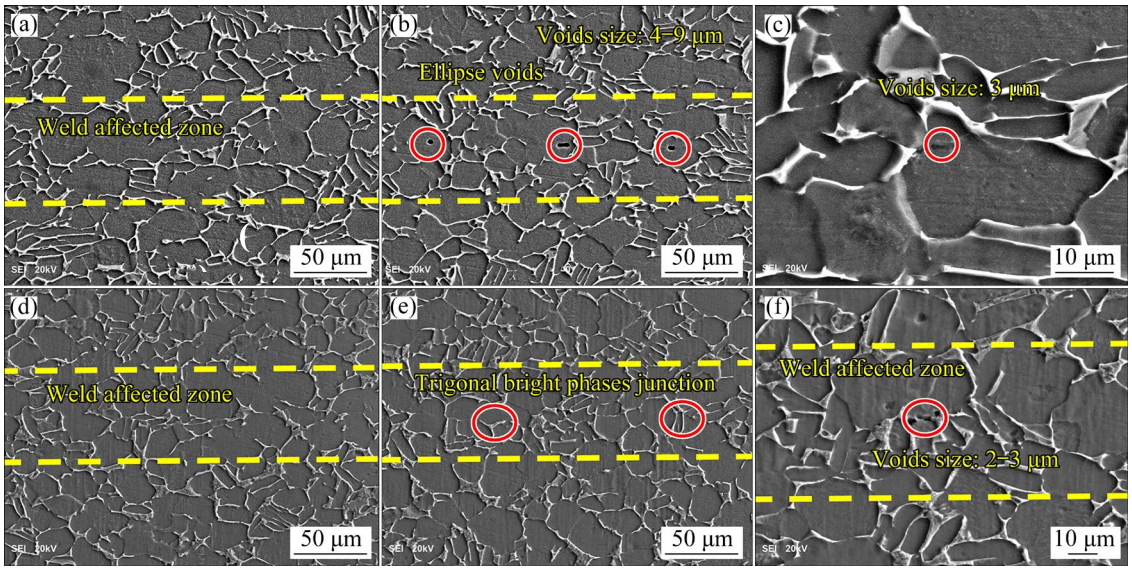

Fig. 10 SEM images of TC4 DB joint under different deformation states with α_s=32°: (a, b, c) AR joint; (d) PWHD1 joint; (e) PWHD2 joint; (f) PWHT joint

PWHD1, PWHD2, and PWHT joints at a bending angle of 32°, respectively. The PWHD1 joint, as shown in Fig. 10(d), generally exhibits very few unbonded areas, which is attributed to the typically small and round shape of the interfacial voids. The DB interface of the PWHD2 joint, as depicted in Fig. 10(e), also shows limited visibility of voids, with some bright phases decorating the bonding lines. In contrast, Fig. 10(f) reveals interfacial voids with irregular edges, which are smaller than those shown in Figs. 10(b, c).

4.3.2 Grain orientation evolution

To better investigate the microstructural differences of the TC4 DB joint under various deformation states, the variations of grain morphology, size, and orientation of the DB interface were analyzed. Figure 11 shows the IPFs in the x–y plane along the y direction (the x and y directions are defined in Fig. 2). By comparing Figs. 11(a) and (d), it is evident that the microstructure of the PWHD1 joint, which has a relatively low bending angle of 17°, is almost consistent with the PWHT joint with a bending angle of 32°. Both joints mainly consist of undeformed grains. As the bending angle increases to 32° for the PWHD1 joint, the blurred and distorted grain boundaries are observed, as shown in Fig. 11(b), which is a typical instability phenomenon during hot deformation. Deformation bands are seen as unstable regions, which are always caused by flow localization [17]. The representative microstructure of the deformation band marked by the box has elongated and fragmented grain characteristics for the PWHD2 joint with a relatively high bending angle (32°), as depicted in Fig. 11(c). It has been noted that the deformation band is usually associated with the activation of the preferred slip system that requires the lowest deformation energy consumption [18]. Similar phenomena have been previously reported in other metals [19]. In addition, there is a significant change in grain orientation, with the ⟨120⟩ crystal orientation dominating in localized areas.

The PFs of the α phase under various deformation states are displayed in Fig. 12. As seen in Figs. 12(a) and (b), the maximum texture intensity of the PWHD1 joint decreases from 4.85 to 3.88 as the bending angle increases from 17° to 32°. In Fig. 12(c), the maximum texture intensity of the PWHD2 joint increases to 4.51, showing a strong local basal texture as the basal poles shift from the x-side to the y-side (Fig. 2). Figure 12(d) indicates that the crystal orientation of the PWHT joint, which is in a stress-free state and has not been deformed, appears relatively random. Overall, texture evolution occurs due to the gradual shift of the grain sliding surface and the sliding direction in the primary deformation direction. This evolution reflects the activation of the grain boundary sliding mechanism during plastic deformation process [20].

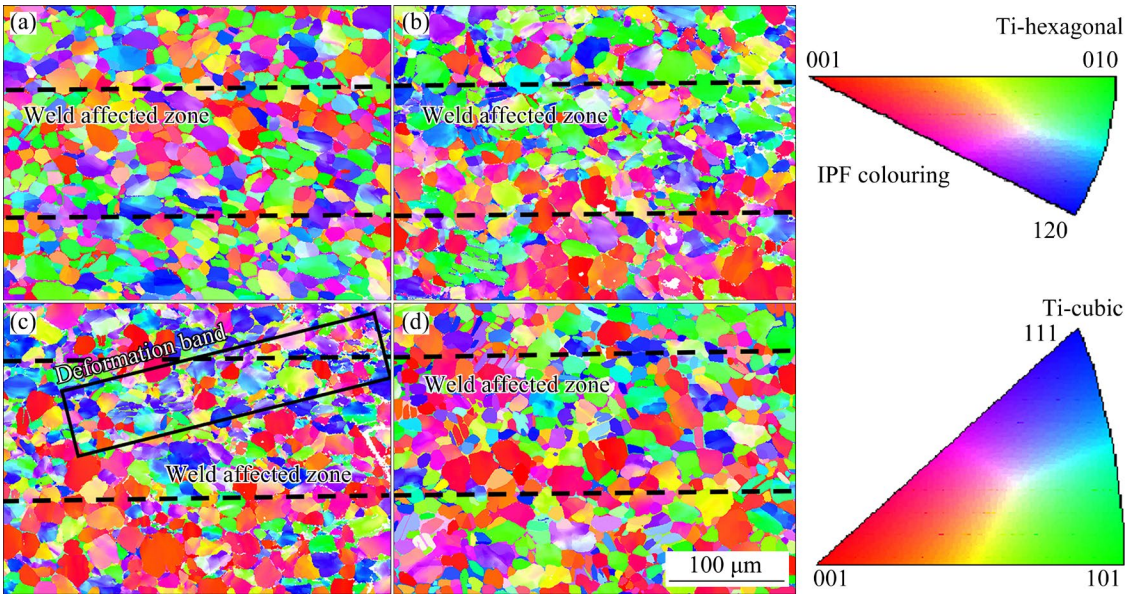

Fig. 11 IPFs of TC4 DB joint under different deformation states: (a) α_s=17°, PWHD1 joint; (b) α_s=32°, PWHD1 joint; (c) α_s=32°, PWHD2 joint; (d) α_s=32°, PWHT joint (Observation along y was applied to IPF triangle)

4.3.3 Slip system

Since the TC4 alloy studied in this work mainly contains the α phase, the slip systems of the α phase are discussed here. It is well known that the high Schmid factor (SF=cos λcos φ) could contribute to grain boundary migration and grain rotation under external stress [21]. In other words, a low SF value indicates that the grains are in the unfavorable slip orientation and appear to be hard grains, while a high SF value indicates that the grains are favorably oriented for slip and appear to be soft grains [22].

Figure 13 shows the average SF values and relative frequencies of high SF values (>0.4) for the basal and primary $\langle a \rangle$ slip systems under different deformation states, respectively. In the primary $\langle a \rangle$ slip system, the average SF values of the PWHD2 and PWHT joints with a bending angle of 32° are less than 0.3, and the relative frequency of SF>0.4 is less than 40%, which is much lower than that of the PWHD1 joint with bending angles of 17° and 32°. In the basal $\langle a \rangle$ slip system, all four types of joints exhibit relatively low average SF values and relative frequency (SF>0.4). The reason for the SF value fluctuations with the change of deformation state is crystallographic orientation evolution resulting from the progressive rotation of adjacent subgrains [23].

4.3.4 Deformation mechanism of primary α phase

The IPFs, GB maps, and LAM maps (Fig. 14) are given to further explain the bending deformation mechanism of the TC4 DB joint. As shown in Fig. 14(b), when the PWHD joint with a small bending angle is subjected to a biaxial stress state, the proportions of the low-angle grain boundaries (LAGBs) represented by the red lines and the high-angle grain boundaries (HAGBs) represented by the green lines are 75.65% and

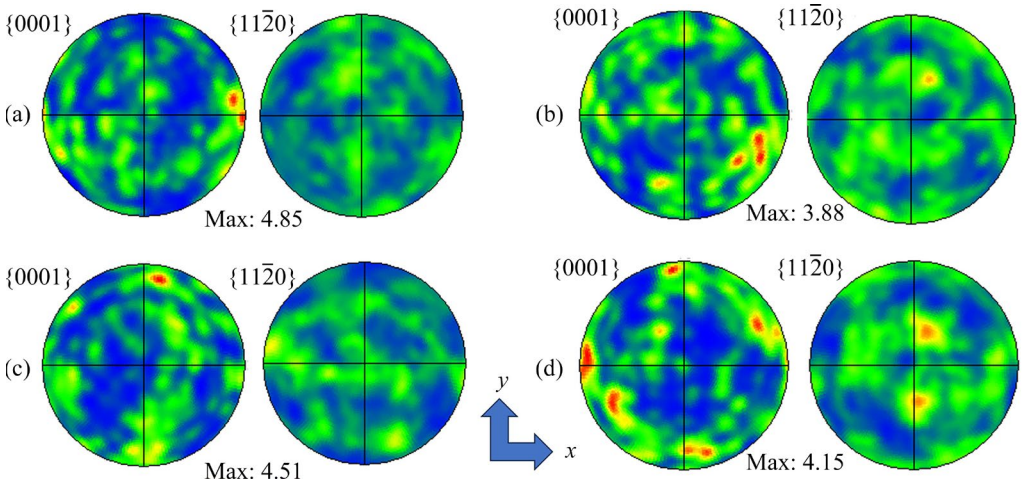

Fig. 12 PFs of TC4 DB joint under different deformation states: (a) α_s=17°, PWHD1 joint; (b) α_s=32°, PWHD1 joint; (c) α_s=32°, PWHD2 joint; (d) α_s=32°, PWHT joint

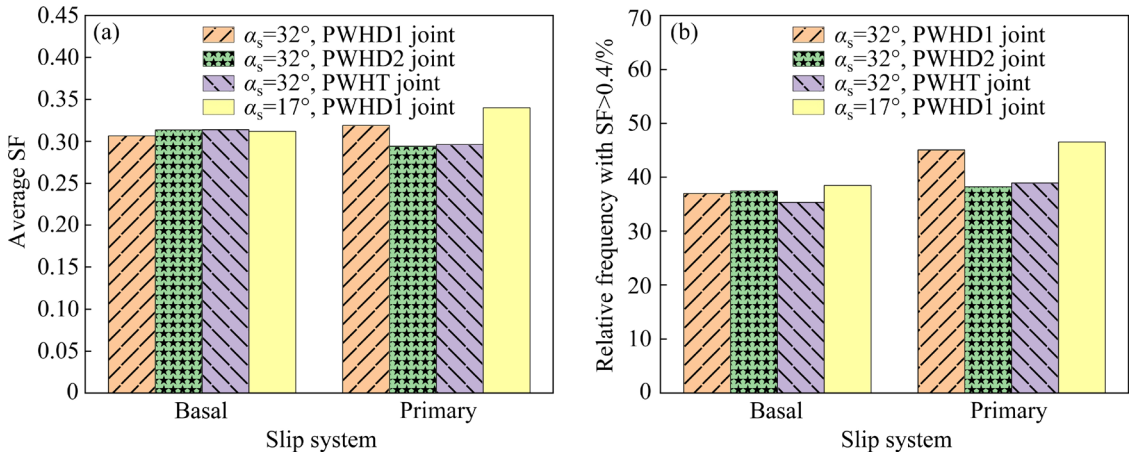

Fig. 13 Statistical analysis of TC4 DB joint under different deformation states: (a) Average SF; (b) Relative frequency with SF >0.4

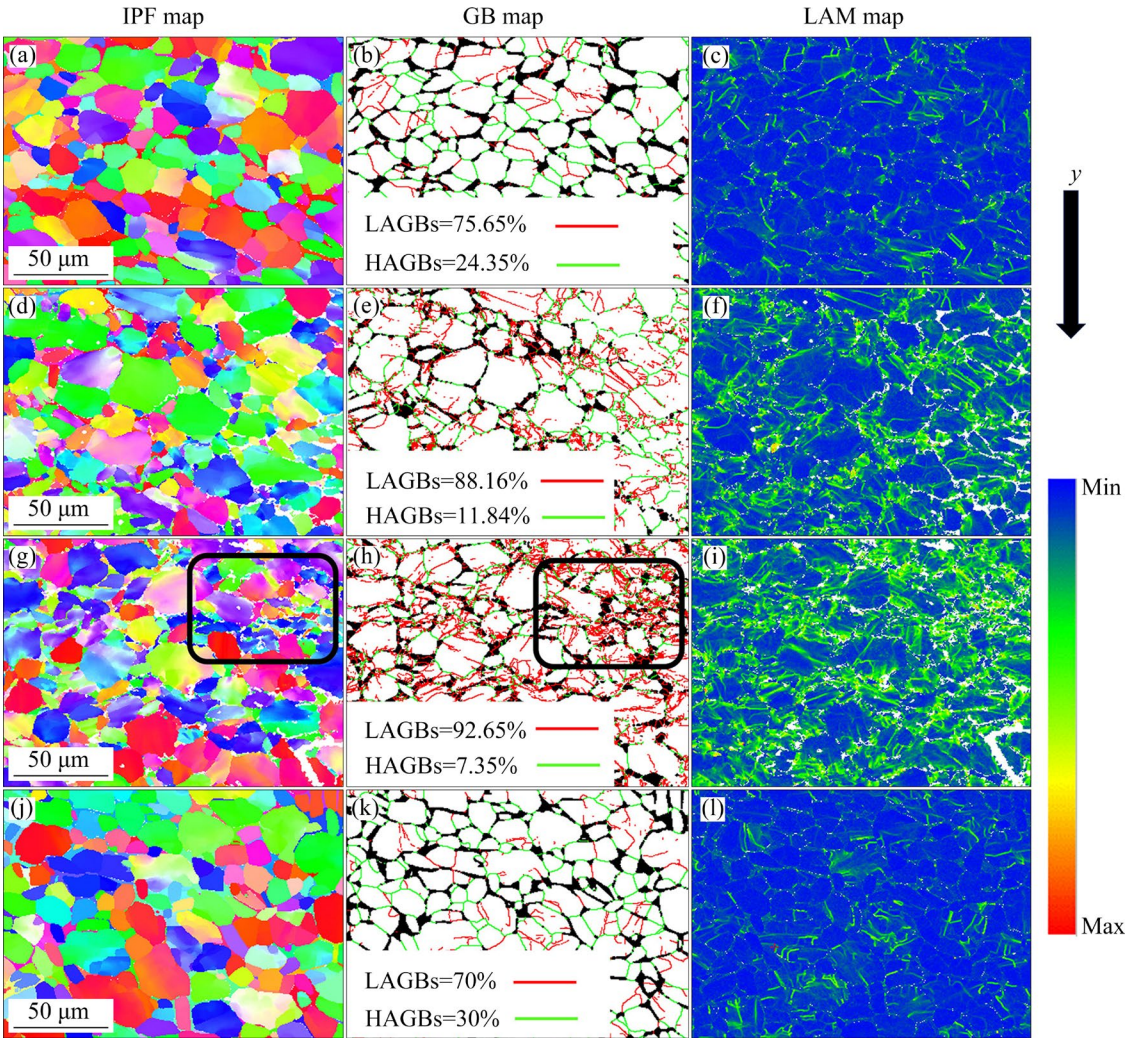

Fig. 14 IPF maps, GB maps, and LAM maps of TC4 DB joint under different deformation states: (a−c) α_s=17°, PWHD1 joint; (d−f) α_s=32°, PWHD1 joint; (g−i) α_s=32°, PWHD2 joint; (j−l) α_s=32°, PWHT joint

24.35%, respectively. As the bending angle increases, the LAGBs proportion of the joint increases to 88.16%, as shown in Fig. 14(e). Figure 14(h) indicates that the LAGBs proportion (92.65%) of the joint under continuous uniaxial stress significantly improves. The PWHT joint has a minimum LAGBs proportion (70%), as shown in Fig. 14(k). It can be found from Figs. 14(e) and (h) that many LAGBs are located within the grains, and the grains are divided into several fine subgrains. Multiple subgrain structures bounded by LAGBs are typical characteristics of dynamic recovery (DRV) [24]. These subgrains can easily convert to new grains with further deformation.

LAM maps can illustrate the plastic strain distribution of crystalline materials and reflect the dislocation density. The PWHD2 joint with a bending angle of 32° shows the highest fraction of the green area representing the higher LAM, implying a higher defect density and higher deformation stored energy. Moreover, the defect distribution within the grains is inhomogeneous and primarily concentrated at the deformation band, as indicated by black rectangles in Figs. 14(g) and (h).

5 Discussion

The bending tests result in local deformation accumulation and the lattice structure distortion of the TC4 DB plate. The bending simulation results indicate three kinds of deformation states in the weld zone. The weld materials of the PWHD1 joint are subjected to biaxial stress. The deformation strain also increases as the bending angle increases from 17° to 32°, as shown in Figs. 14(c) and (f). The weld materials of the PWHD2 joint maintain

the uniaxial deformation state, causing the highest dislocation density and deformation strain. Such stress partitioning characteristics result in tensile properties partitioning. The PWHD2 joint has the highest ultimate tensile strength, followed by the PWHT joint and the PWHD1 joint.

During the deformation process, some dislocations migrate to grain boundaries and vanish, while others plug and entangle. The final dislocation density depends on the competition between the two mechanisms. A higher dislocation density makes it more difficult for slip to begin [25]. The LAGBs gradually developed from α/β grain boundaries into grains interior, indicating the development of the DRV process. In addition, as shown in Figs. 14(h) and (i), the green stripes in the LAM map coincide with LAGBs. The LAGBs can act as nucleation sites for new grains during the subsequent dynamic recrystallization (DRX) process. The conversion of subgrain boundaries from LAGBs to HAGBs consumes many dislocations and results in the refinement of the original structure. The DRV grains do not have enough time to transform due to the relatively low temperature of 750 °C. So, many new dislocations are maintained, causing a high dislocation density under an inadequate DRV process.

The relatively low SF value in the main slip systems indicates an unfavorable slip orientation in the main slip system of the PWHT joint. From the above analysis, it has been proven that the mechanical properties of the DB joint can be improved by applying appropriate deformation states to the DB interface during hot bending. The significant accumulation of LAGBS and dislocations for the joint, under a uniaxial stress state characterized by continuous tangential tension and radial compression deformation, is the main reason for the better mechanical properties following hot bending.

6 Conclusions

(1) Three types of deformation states were obtained in the weld zone for the TC4 DB joint by hot bending, including the stress-free state without deformation, the uniaxial stress state with only tangential tension or radial compression, and the biaxial stress state with radial compression/ tangential tension or radial tension/tangential compression.

(2) The joint under the uniaxial stress state in the weld zone showed the highest ultimate tensile strength. This enhancement is attributed to texture strengthening in the basal {0001} planes, resulting from the gradual shift of grain sliding surface and sliding direction, as well as the presence of deformation bands in the joint.

(3) Microstructural analyses confirmed that the significant accumulation of dislocation density and LAGBS in the grains are the main reasons for the improvement in mechanical properties of the joint under the uniaxial stress state, which caused the relatively low SF value in the primary $\langle a \rangle$ slip systems.

(4) The texture randomization was found in the joint under the stress-free state without deformation. The joint showed a higher tensile strength compared to that under biaxial stress conditions. Although few dislocations and LAGBS existed in the joint under the stress-free state, the unfavorable slip orientation in the main slip system was confirmed.

CRediT authorship contribution statement

Can LI: Conceptualization, Methodology, Investigation, Formal analysis, Data curation, Original draft preparation; **Yong LI:** Writing − Review & editing, Supervision, Funding acquisition; **De-xin ZHANG:** Data curation; **Yan-qiang XU:** Validation; **Xiao-xing LI:** Writing − Review & editing; **Guang-lu MA:** Visualization.

Declaration of competing interest

The authors declare that they have no known competing financial interests or personal relationships that could have appeared to influence the work reported in this paper.

Acknowledgments

The authors would like to thank the financial support from Fundamental Research Funds for the Central Universities, China (No. YWF-23-L-1012), and the National Natural Science Foundation of China (No. 52005020).

References

[1] XIONG J T, SUN J R, WANG J C, ZHANG H, SHI J M, LI J L, WANG J C. Evaluation of the bonded ratio of TC4 diffusion bonded joints based on ultrasonic C-scan [J]. Journal of Manufacturing Processes, 2019, 47: 238−243.

[2] LEI Yi-wen, MA Guang-lu, LIU Yue, ZHAO Wei, WU Hui-ping, LI Xi-feng. Vibration fatigue properties and deterioration mechanism of diffusion bonded TC4 titanium alloy [J]. Transactions of Nonferrous Metals Society of China, 2024, 34(2): 533−546.

[3] LI Can, LI Yong, ZHANG De-xin, LI Xiao-xing, ZHAO Wan-Qi. Experimental investigation of the mechanical properties and microstructures of Ti−6Al−4V solid-state diffusion bonding joint under high temperature conditions [J]. Journal of Materials Research and Technology, 2023, 26: 4042−4058.

[4] LI Zhao-xi, LI Shi-wei, PENG Yu, ZHANG Yan-min, GUO Wei, XIONG Jiang-tao, LI Jing-long. Fracture behavior and mechanical properties of Ti−6Al−4V joints diffusion-bonded with pre-designed interfacial voids [J]. Journal of Manufacturing Processes, 2022, 84: 1331−1338.

[5] XU Wei-feng, MA Jun, LUO Yu-xuan, FANG Yue-xiao. Microstructure and high-temperature mechanical properties of laser beam welded TC4/TA15 dissimilar titanium alloy joints [J]. Transactions of Nonferrous Metals Society of China, 2020, 30(1): 160−170.

[6] ZHANG Hao, LI Jing-long, MA Ping-yi, XIONG Jiang-tao, ZHANG Fu-sheng. Study on microstructure and impact toughness of TC4 titanium alloy diffusion bonding joint [J]. Vacuum, 2018, 152: 272−277.

[7] DZIADOŃ A, MUSIAŁ E. Effects of post-weld heat treatment on the microstructure and mechanical properties of the AZ91 laser welded joint [J]. Archives of Metallurgy and Materials, 2021, 67(2): 435−440.

[8] LI Can, SARDAR MUHAMMAD I, LANG Li-hui, GUO Ying-jian, LI Xiao-xing, ALEXANDROVA S, ZHANG De-xin. Hot deformation behavior and strain compensation constitutive model of equiaxed fine grain diffusion-welded micro-duplex TC4 titanium alloy [J]. Chinese Journal of Aeronautics, 2023, 36(4): 510−522.

[9] JIANG Yuan-bo, LI Cheng-ning, WANG Dong-po, LIU Jiang-cheng, LI Ye-zheng, DI Xin-jie. The mutual effect of hydrogen and cyclic plastic deformation on ductility degradation of X65 reeled-pipeline welded joint [J]. Materials Science and Engineering: A, 2020, 791: 139739.

[10] TANG Bin, WANG W Y, ZHU Lei, KOU Hong-chao, LI Jin-shan. Hot deformation study and interface characterization for TiAl/Ti_2AlNb diffusion bonds based on the serial constitutive model [J]. Intermetallics, 2019, 104: 66−73.

[11] TAN L J, YAO Z K, NING Y Q, GUO H Z. Effect of isothermal deformation on microstructure and properties of electron beam welded joint of Ti_2AlNb/TC11 [J]. Materials Science and Technology, 2011, 27(9): 1469−1474.

[12] LIU Zhe, XIN Ren-long, WU Xia, LIU De-jia, LIU Qing. Improvement in the strength of friction-stir-welded ZK60 alloys via post-weld compression and aging treatment [J]. Materials Science and Engineering: A, 2018, 712: 493−501.

[13] ZHU Lei, TANG Bin, WEI Bei-bei, DING Ming-xuan, ZOU Cheng-xiong, LIU Yan, ZHENG Guo-ming, LI Jin-shan. Strengthening mechanisms of TiAl/Ti_2AlNb diffusion bonding joint after post-bonded heat treatment and hot deformation [J]. Materials Science and Engineering: A, 2021, 825: 141872.

[14] WAN Yu, JIANG Wen-chun, LI Hai-gang. Cold bending effect on residual stress, microstructure and mechanical properties of Type 316L stainless steel welded joint [J]. Engineering Failure Analysis, 2020, 117: 104825.

[15] CRAFOORD R. Plastic sheet bending [D]. Sweden, Gothenburg: Chalmers University of Technology, 1970.

[16] MA Li-xia, WAN Min, LI Wei-dong, SHAO Jie, HAN Xiao-ning, ZHANG Ji-chun. On the superplastic deformation mechanisms of near-α TNW700 titanium alloy [J]. Journal of Materials Science & Technology, 2022, 108: 173−185.

[17] LI Cheng-lin, NARAYANA P L, REDDY N S, CHOI S W, YEOM J T, HONG J K, PARK C H. Modeling hot deformation behavior of low-cost Ti−2Al−9.2Mo−2Fe beta titanium alloy using a deep neural network [J]. Journal of Materials Science & Technology, 2019, 35: 907−916.

[18] JANDAGHI M R, POURALIAKBAR H. Study on the effect of post-annealing on the microstructural evolutions and mechanical properties of rolled CGPed aluminum−manganese−silicon alloy [J]. Materials Science and Engineering: A, 2017, 679: 493−503.

[19] LI Chang-min, HUANG Liang, ZHAO Ming-jie, GUO Shi-qi, LI Jian-jun. Hot deformation behavior and mechanism of a new metastable β titanium alloy Ti−6Cr−5Mo−5V−4Al in single phase region [J]. Materials Science and Engineering: A, 2021, 814: 141231.

[20] YASMEEN T, ZHAO Bing, ZHENG Jing-hua, TIAN Fa-min, LIN Jian-guo, JIANG Jun. The study of flow behavior and governing mechanisms of a titanium alloy during superplastic forming [J]. Materials Science and Engineering: A, 2020, 788: 139482.

[21] LIU Zhang-guang, LI Pei-jie, XIONG Liang-tong, LIU Tai-ying, HE Liang-ju. High-temperature tensile deformation behavior and microstructure evolution of Ti55 titanium alloy [J]. Materials Science and Engineering: A, 2017, 680: 259−269.

[22] WAN V V C, CUDDIHY M A, JIANG J, MACLACHLAN D W, DUNNE F P E. An HR-EBSD and computational crystal plasticity investigation of microstructural stress distributions and fatigue hotspots in polycrystalline copper [J]. Acta Materialia, 2016, 115: 45−57.

[23] SUN Yong-gang, ZHANG Chang-jiang, FENG Hong, ZHANG Shu-zhi, HAN Jian-chao, ZHANG Wang-gang, ZHAO Er-tuan, WANG Hong-wei. Dynamic recrystallization mechanism and improved mechanical properties of a near α high temperature titanium alloy processed by severe plastic deformation [J]. Materials Characterization, 2020, 163: 110281.

[24] HUANG K, LOGÉ R E. A review of dynamic recrystallization phenomena in metallic materials [J]. Materials & Design, 2016, 111: 548−574.

[25] CHEN Dong, YANG Qian-ru, YANG Na-chuan, WANG Meng, XU Qiang, WU Jing-yuan, JIANG Yan-bin, LI Zhou, XIAO Zhu, WEI Hai-gen. Hot compressive deformation and microstructural evolution of 60NiTi alloy [J]. Transactions of Nonferrous Metals Society of China, 2023, 33(1): 189−200.

热弯曲变形状态对扩散连接 TC4 合金显微组织和力学性能演变的影响

李 灿[1]，李 勇[1]，张德鑫[1]，徐彦强[2]，李晓星[1]，马广璐[2]

1. 北京航空航天大学 机械工程及自动化学院，北京 100191；
2. 沈阳黎明航空发动机有限责任公司，沈阳 110043

摘 要：通过厚板热弯曲研究不同热变形状态对扩散连接 TC4 合金显微组织和力学性能演变的影响。当弯曲温度为 750 ℃、弯曲角度分别为 17°和 32°时，通过有限元模拟获得了厚板的变形状态，分析了扩散连接界面的显微组织和力学性能。在单轴应力状态下的接头具有最高的极限抗拉强度，这是由位错密度和晶粒内小角度晶界的大量积累造成的。实验结果还揭示了基面{0001}织构强化以及主滑移系沿变形方向相对较低的施密德因子值。无应力状态下的接头存在不利于变形的滑移方向，极限抗拉强度高于双轴应力状态下的接头。

关键词：扩散连接接头；厚板；热弯曲；应力状态；拉伸强度

(Edited by Xiang-qun LI)